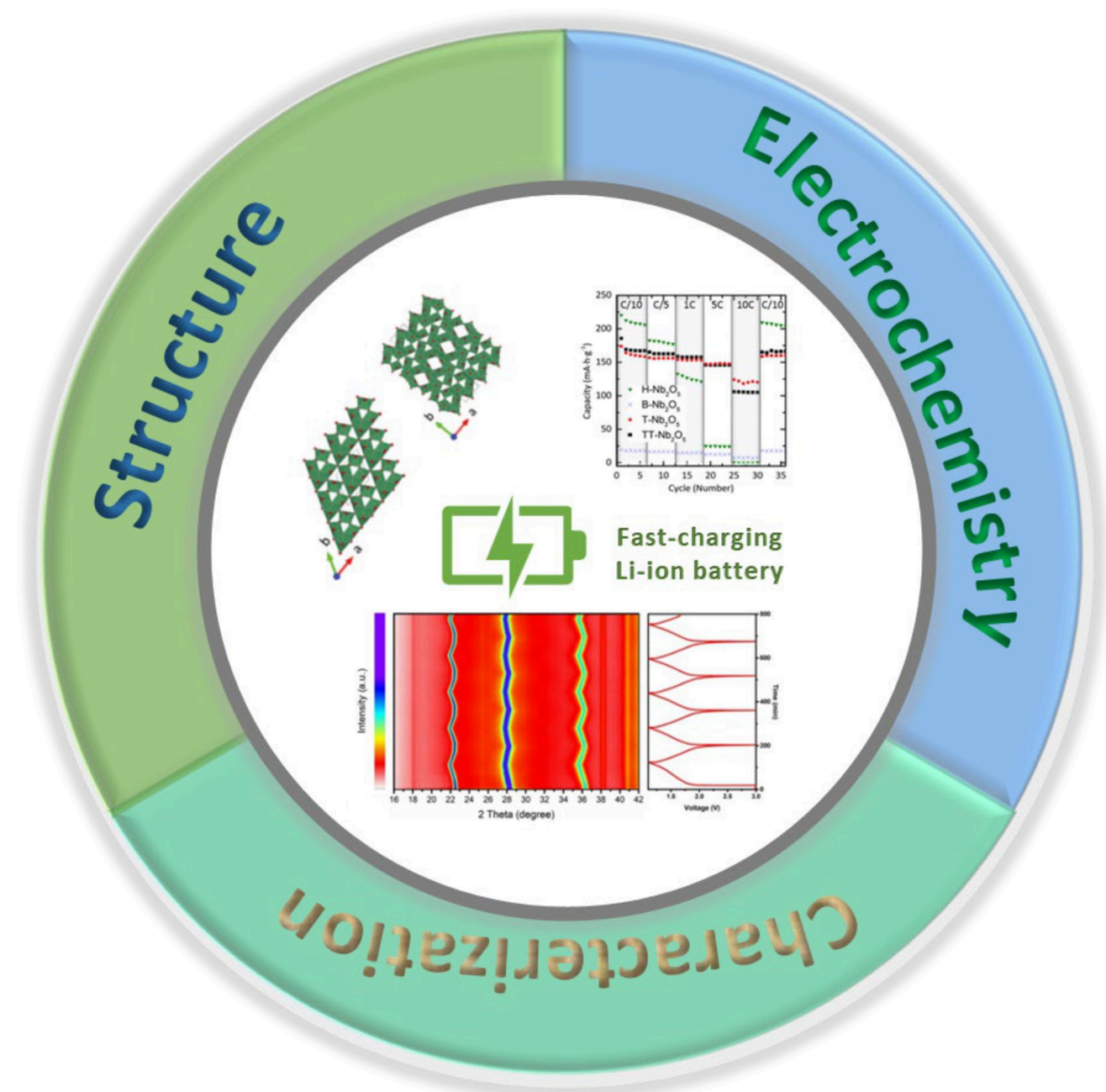# Probing the Electrochemical Processes of Niobium Pentoxides (Nb$_2$O$_5$) for High-Rate Lithium-ion Batteries: A Review

Jie Lin[+, a, b] Siyu Zhao[+, a, c, d] Rhodri Jervis,*[a, c] and Paul Shearing*[a, c, d]

The rising demand to electrify power-intensive energy devices and systems, as well as fast charging, has imposed a great challenge in current chemistries for lithium-ion batteries (LIBs), whose rate capabilities are predominantly restricted by the conventional graphite anode. Niobium pentoxide (Nb_2O_5) is a promising high-rate anode material for LIBs with extraordinary rate performance beyond 5 C and good theoretical capacity (~202 mAh·g^{-1}). With many possible crystal structures, Nb_2O_5 has a complicated family of different polymorphs, each of which can possess distinct electrochemical properties, specific capacity, cycling stability, and rate capability. This special feature of Nb_2O_5 makes it a challenging material to understand and requires a comprehensive investigation of every one of its polymorphs. In this paper, we summarize the state-of-the-art research on Nb_2O_5 polymorphs for LIBs, with an emphasis on the advanced characterisation techniques that have been used to probe the electrochemical processes of Nb_2O_5. Key findings related to Nb_2O_5 that have emerged from the previous studies are highlighted, and new scientific questions that are important for its scale-up and commercialization are proposed for future research.

1. Introduction

Battery energy storage is a key enabler of the energy transition from fossil fuels to clean and sustainable renewable energy sources, to address pressing environmental challenges such as climate change, air pollution, and resource depletion.[1,2] It is crucial to the growth of electric vehicles and the integration of renewable energy into grid networks, as well as the potential for vehicle-to-grid interactions, which helps to create a more flexible, resilient, and sustainable energy system.

Owing to the rapid progress in battery chemistries, cell manufacturing and battery management, lithium-ion batteries (LIBs) have superior energy capacity, cycle life, electrochemical stability window over other conventional (e.g., lead-acid, nickel metal hydride) and novel rechargeable batteries (e.g., sodium-ion, zinc-ion),[3–5] and are currently the most efficient, reliable, and economical battery technologies for consumer electronics, electric vehicles, and grid-scale energy storage.[6,7] However, the rising demand for battery power to electrify more devices and systems (e.g., unmanned aerial vehicles and aeroplanes), as well as the essential need for fast charging, has imposed greater challenges on the existing battery chemistries. Commercial LIBs mostly adopt a graphite (possibly blended with silicon/SiO_x) anode, which operates in a voltage window of ~0.01–1.0 V vs. Li/Li$^+$. In this low voltage range, LIBs are subject to electrolyte decomposition, solid electrolyte interphase (SEI) growth, and dendrite formation, which are inclined to occur at high currents and thus limit their rate capability and cycle life.[8–10] The solid-state diffusion of Li ions in graphite material is also unfavourable for fast lithium intercalation. To tackle this problem, novel high-rate anode materials are being investigated and developed.

Niobium pentoxide (Nb_2O_5) is a promising material for fast lithium intercalation. It operates at a high voltage window between 1.0 and 3.0 V vs. Li/Li$^+$, during which the formation of lithium dendrite and SEI layer can be suppressed.[11] It has a theoretical capacity of ~202 mAh·g^{-1}, higher than that of the widely deployed lithium-titanium-oxide ($Li_4Ti_5O_{12}$ or LTO) at 175 mAh·g^{-1}.[12] Nb_2O_5 is also considered to be non-toxic[13] and can be synthesized using many different low-cost methods[14,15] with the relatively abundant resource of niobium (Nb).

On the other hand, Nb_2O_5 is a complex material and contains about 15 different polymorphs with various crystal structures. Several of them, have been commonly investigated for battery applications, including TT–, T–, M–, B– and H–Nb_2O_5. The prefixes of the polymorphs are nominated by Schäfer et al.[16] in German, based on either the synthesis temperature (see Figure 1), e.g., TT (tief-tief, i.e., low-low), T (tief), M (medium) and H (hoch, i.e., high) or particle shapes, e.g., B (blätter, i.e., leaves/plates). The different polymorphs of Nb_2O_5 can exhibit distinct physical and electrochemical properties, specific capacity, cycling stability, and rate capability.[15]

T–Nb_2O_5 is from the *Pbam* space group with an orthorhombic structure and lattice parameters of a = 6.175 Å, b = 29.175 Å, and c = 3.93 Å (see Table 1).[17] This polymorph can be obtained at low annealing temperature (e.g., 550–750 °C). T–Nb_2O_5 allows fast lithium intercalation, and its crystal structure remains unchanged after lithiation.[18] Consequently, it possesses excellent rate capability and cycling stability, and is the most commonly studied for battery applications.[11,14,19]

The crystal structure of TT–Nb_2O_5 has not been completely refined, so it has been described as a pseudo-hexagonal or monoclinic crystal structure. It is widely accepted that the unit cell of TT–Nb_2O_5 falls in the space group of *P6/mmm* with lattice parameters a = b = 3.607 Å and c = 3.925 Å.[20,21] Obtained at about 300 °C annealing temperature, this polymorph is metastable and stabilized as a result of oxygen vacancies or OH$^-$ and Cl$^-$ impurities.[14,15] TT–Nb_2O_5 is deemed as a disordered phase of T–Nb_2O_5 and it remains a single phase during (de)lithiation.

[a] Dr. J. Lin,$^+$ Dr. S. Zhao,$^+$ Dr. R. Jervis, Prof. P. Shearing
The Electrochemical Innovation Lab, Department of Chemical Engineering, University College London, London WC1E 6BT, United Kingdom
E-mail: rhodri.jervis@ucl.ac.uk
paul.shearing@eng.ox.ac.uk

[b] Dr. J. Lin$^+$
School of Mechanical and Aerospace Engineering, Queen's University Belfast, Ashby Building, Stranmillis Road, Belfast BT9 5AH, United Kingdom

[c] Dr. S. Zhao,$^+$ Dr. R. Jervis, Prof. P. Shearing
The Faraday Institution, Harwell Campus, Didcot, OX11 0RA, United Kingdom

[d] Dr. S. Zhao,$^+$ Prof. P. Shearing
Department of Engineering Science, University of Oxford, Parks Road, Oxford, OX1 3PJ, UK

[$^+$] These authors contributed equally

ChemElectroChem

Review

doi.org/10.1002/celc.202300581

Chemistry Europe
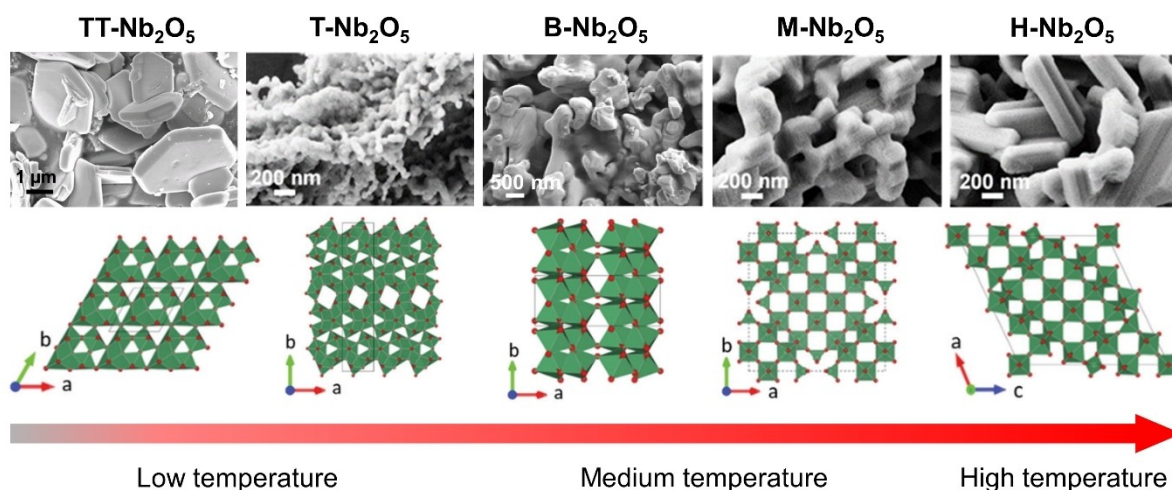European Chemical
Societies Publishing

Figure 1. Morphology and crystal structure of different Nb_2O_5 polymorphs. Reproduced from Ref. [12,27,28]. Copyright (2016, 2021, 2023), with permissions from American Chemical Society and Elsevier.

Table 1. Crystal structural characteristics of different Nb_2O_5 polymorphs.					
Polymorph	Structure	Lattice parameters	Space group	Point group	Ref
TT	Pseudohexagonal	a = 3.607 Å c = 3.925 Å	P6/mmm	–	[20,21]
T	Orthorhombic	a = 6.175 Å b = 29.175 Å c = 3.930 Å α = 90.000° β = 90.000° γ = 90.000°	Pbam	D_{2h}^{9}	[17]
B	Monoclinic	a = 12.740 Å b = 4.883 Å c = 5.561 Å α = 90.000° β = 105.020° γ = 90.000°	C2/c	C_{2h}^{6}	[22,23]
M	Tetragonal	a = 20.440 Å b = 20.440 Å c = 3.832 Å α = 90.000° β = 90.000° γ = 90.000°	I4/mmm	D_{4h}^{17}	[24]
H	Monoclinic	a = 21.153 Å b = 3.823 Å c = 19.356 Å α = 90.000° β = 119.800° γ = 90.000°	P2/m	C_{2h}^{1}	[25,26]

B–Nb_2O_5 falls in the *C2/c* space group with a monoclinic structure and lattice parameters of a = 12.740 Å, b = 4.883 Å, c = 5.561 Å and β = 105.020°.[22,23] This polymorph is synthesized at medium temperature range of 650–950 °C.

M–Nb_2O_5 is another medium-temperature phase (650–950 °C) of Nb_2O_5. It has a tetragonal crystal structure in the *I4/mmm* space group with lattice parameters a = 20.440 Å, c = 3.832 Å.[24]

H–Nb_2O_5 is in the space group *P2/m* with a monoclinic structure. a = 21.153 Å, b = 3.823 Å, c = 19.356 Å, and β = 119.8°.[25] Obtained at the highest temperature (> 950 °C), this

polymorph is the most thermodynamically stable. H–Nb_2O_5 has many tunnel-like channels which offers ideal pathways for Li diffusion with low hindrance, and it will undergo a phase change during lithiation.[26]

A summary of the morphology and crystal structure of different polymorphs are provided in Figure 1 and Table 1.

In this paper, we provide a comprehensive summary of the crystal structures and their corresponding electrochemical performance for a wide range of Nb_2O_5 polymorphs that are commonly investigated for electrochemical energy storage. More importantly, we highlight the experimental observations

ChemElectroChem

Review
doi.org/10.1002/celc.202300581

Chemistry
Europe
European Chemical
Societies Publishing

of Nb_2O_5 from typical characterisation techniques, such as electron microscopy, X-ray methods, and Raman spectroscopy, to shed light on existing findings of their structural, chemical, and electrochemical behaviours. Building upon the current research progress of Nb_2O_5, more research efforts are required to accelerate the development and commercialization of Nb_2O_5 for battery applications.

2. Electrochemical performance

Similar to other transition metal oxides like $LiCoO_2$ and $LiMn_2O_4$, lithium ions can be reversibly intercalated into the crystal structure of Nb_2O_5, and the electrochemical reactions of Nb_2O_5 during lithiation and delithiation can be written as:

$$Nb_2O_5 + xLi^+ + xe^- \rightleftharpoons Li_xNb_2O_5 \qquad (1)$$
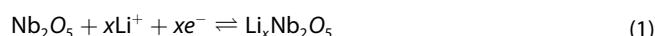
where the maximum lithium stoichiometry (x_{max}) of $Li_xNb_2O_5$ is 2.

The theoretical capacity (Q_{th}) of Nb_2O_5 can be calculated based on Faradaic charge transfer as follows:

$$Q_{th} = \frac{nF}{M_w} = \frac{2 \times 96485.3 \text{ C/mol}}{265.8 \text{ g/mol}} = \qquad (2)$$
$$726.0 \text{ C/g} = 201.7 \text{ mAh/g}$$

where F is the Faraday constant, M_w is the molar weight of Nb_2O_5.

The electrochemical performance of the different phases of Nb_2O_5 in lithium-ion batteries varies depending on their crystal structure, morphology, and synthesis method. The behaviours of different Nb_2O_5 can be easily revealed by their cyclic voltammetry (CV) and open-circuit potential (OCP) with reference to a lithium counter electrode. Typical examples[27,28] of CV and OCP for TT−, T−, B−, M−, and H−Nb_2O_5 are shown in Figure 2. A significant difference between low-temperature and medium/high-temperature Nb_2O_5 can be found on the CV curves, where the both the cathodic and anodic current can span a wide voltage window in TT− and T−Nb_2O_5, but concentrate on several characteristic peaks in B−, M−, and H−Nb_2O_5. This result indicates that the Nb_2O_5 polymorphs can be dominated by different charge storage mechanisms. In general, the major charge storage mechanisms in electrochemical devices include the diffusion-controlled insertion process via Faradaic reaction and surface-controlled capacitive effects including pseudocapacitance and double-layer capacitance, which lead to distinct battery-like or capacitor-like behaviours, respectively.[29]

It is commonly acknowledged that T−Nb_2O_5 has a unique charge storage mechanism as intercalation pseudo-capacitance, which promotes fast two-dimensional (2D) lithium diffusion within its crystal structure and exhibits a strong capacitive effect.[30,31] The similarity between TT− and T−Nb_2O_5 infers the former may have the same feature as a disordered phase of T−Nb_2O_5. In contrast, B−, M−, and H−Nb_2O_5 remain as traditional

battery materials whose charge transfer are controlled solely by lithium diffusion.

The electrochemical processes probed from CV can be further supported by their OCP vs. Li^+/Li. After an initial voltage drop, TT− and T−Nb_2O_5 have a linear OCP with state-of-lithiation (SOL), whereas M− and H−Nb_2O_5 show clear voltage plateaus at certain SOLs. The voltage plateau is usually a sign of phase transition, which infers a structural change of the material's crystal during lithiation. The lithiation of TT− and T−Nb_2O_5 imposes no phase change but volume expansion of their lattices.[18] In addition, B−Nb_2O_5 exhibits poor electrochemical performance with limited capacity for lithium storage, despite it showing clear redox peaks in CV.[28]

Beyond the charge storage mechanisms, charge capacity, rate capability and cycle life are the important electrochemical performance for different Nb_2O_5 polymorphs, which can affect their feasibility in various applications. Galvanostatic charge-discharge tests are essential techniques to examine the rate capability and cyclability of Nb_2O_5. In these tests, a "C-rate" is often used to specify the test condition of the applied current, in addition to the current density in $A g^{-1}$, which is the amount of time in hours required to fully charge/discharge the material with reference to its theoretical capacity. Typical examples[27,28] of the rate capability and cyclability tests of different Nb_2O_5 polymorphs are shown in Figure 3. Owing to the lithium insertion process in M- and H−Nb_2O_5, they present higher charge capacity at lower C-rates but experience a large capacity drop at higher C-rates (≥ 5 C) due to their limited Li^+ diffusivity. In contrast, the distinct pseudocapacitance mechanism in TT- and T−Nb_2O_5 enables excellent capacity retention at ultrafast C-rates beyond 10 C, despite them providing relatively lower initial capacities at low C-rates.

The cycle life of the Nb_2O_5 polymorphs is also found to be highly relevant to their charge storage mechanisms. The phase transition in the M− and H−Nb_2O_5 during (de)lithiation can cause irreversible structural changes and defects in their crystals, and lead to faster degradation and capacity fade. The capacitive effects in TT− and T−Nb_2O_5 promotes fast lithium diffusion while not altering their crystal structures, hence ensuring great stability over continuous cycles.

Despite that some Nb_2O_5 polymorphs allow fast Li diffusion, one common issue faced by Nb_2O_5 crystals is their poor electrical conductivity for electrons that is closed to an insulator or semiconductor. A wide range of the electrical conductivity between the order of 10^{-6} and 10^{-13} $S cm^{-1}$ has been reported for different Nb_2O_5 polymorphs,[32] and even for the same polymorph, the result was inconsistent when different synthesis methods were employed.[33] In general, H−Nb_2O_5 is known to be more conductive than other polymorphs with a common conductivity value of 3.0×10^{-6} $S cm^{-1}$.[20,34,35] The poor conductivity can severely increase the impedance and restricts the rate capability of thick Nb_2O_5 electrodes. Therefore, a few research efforts have been made to improve the electrical conductivity of Nb_2O_5 electrodes, and typical solutions include designing diverse Nb_2O_5 nanostructures (e.g., nanobelts, nanosheets, nanoparticles) and integrating Nb_2O_5 crystals with carbon as composite electrodes. One example was given by Meng et al.[36]
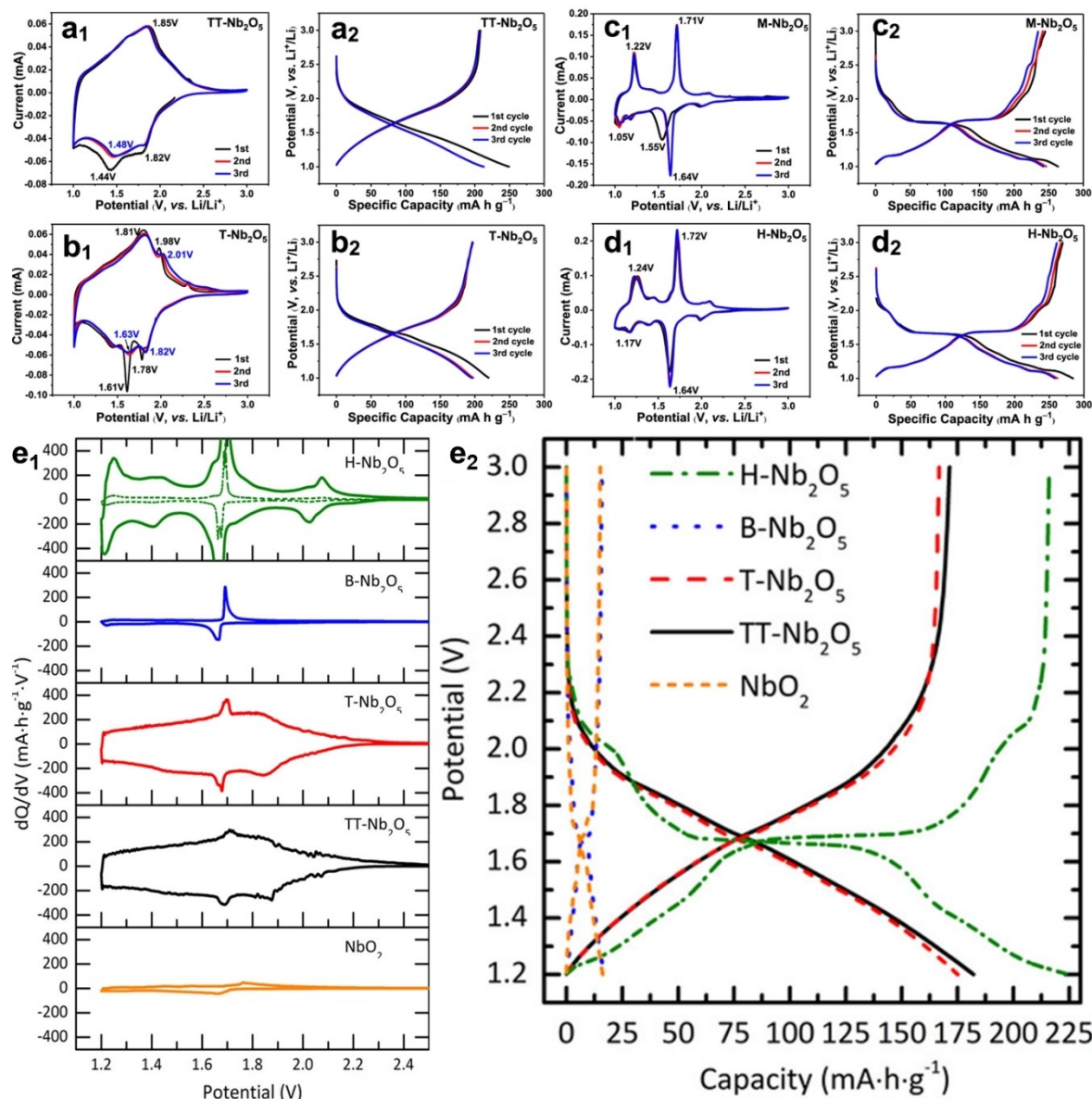
ChemElectroChem

Review
doi.org/10.1002/celc.202300581

**Chemistry
Europe**
European Chemical
Societies Publishing

Figure 2. Cyclic voltammetry and first three galvanostatic discharge-charge (GCD) cycles of (a_1, a_2) TT–Nb_2O_5, (b_1, b_2) T–Nb_2O_5, (c_1, c_2) M–Nb_2O_5, (d_1, d_2) H–Nb_2O_5 from 3.0 to 1.0 V at 10/C applied current. Reproduced from Ref. [27]. Copyright (2021), with permissions from American Chemical Society. (e_1) Differential capacity analyses from the discharge-charge cycles in (e_2) galvanostatic discharge-charge curves for NbO_2 and TT–, T–, B–, and H–Nb_2O5 polymorphs from 3.0 to 1.2 V at C/10 applied current. Reproduced from Ref. [28]. Copyright (2016), with permissions from American Chemical Society.

where they constructed carbon-confined Nb_2O_5 nanoparticles (TT–Nb_2O_5@C, T–Nb_2O_5@C, H–Nb_2O_5@C) via a mismatched coordination reaction, as shown in Figure 4. The obtained materials presented high surface area, high conductivity and short diffusion length for charge transfer and storage, hence exhibited remarkable rate performance and cycling stability. A comprehensive summary of the charge capacity and rate performance of different Nb_2O_5 polymorphs tested by different researchers are listed in Table 2.

3. Characterisation methods

To investigate the physical and chemical properties of the materials, adoption of proper characterisation methods is important to obtain an accurate understanding of the electrodes. When combined with specially designed sample preparation methods or *in situ/operando* cells, these characterisation techniques could be further used to study the charge-transfer mechanisms and degradation mechanisms, which is of importance to provide insights into future electrode design and improvement. Herein, a selection of commonly used characterisation techniques is summarized in Table 3 and these techniques will be introduced with some examples.
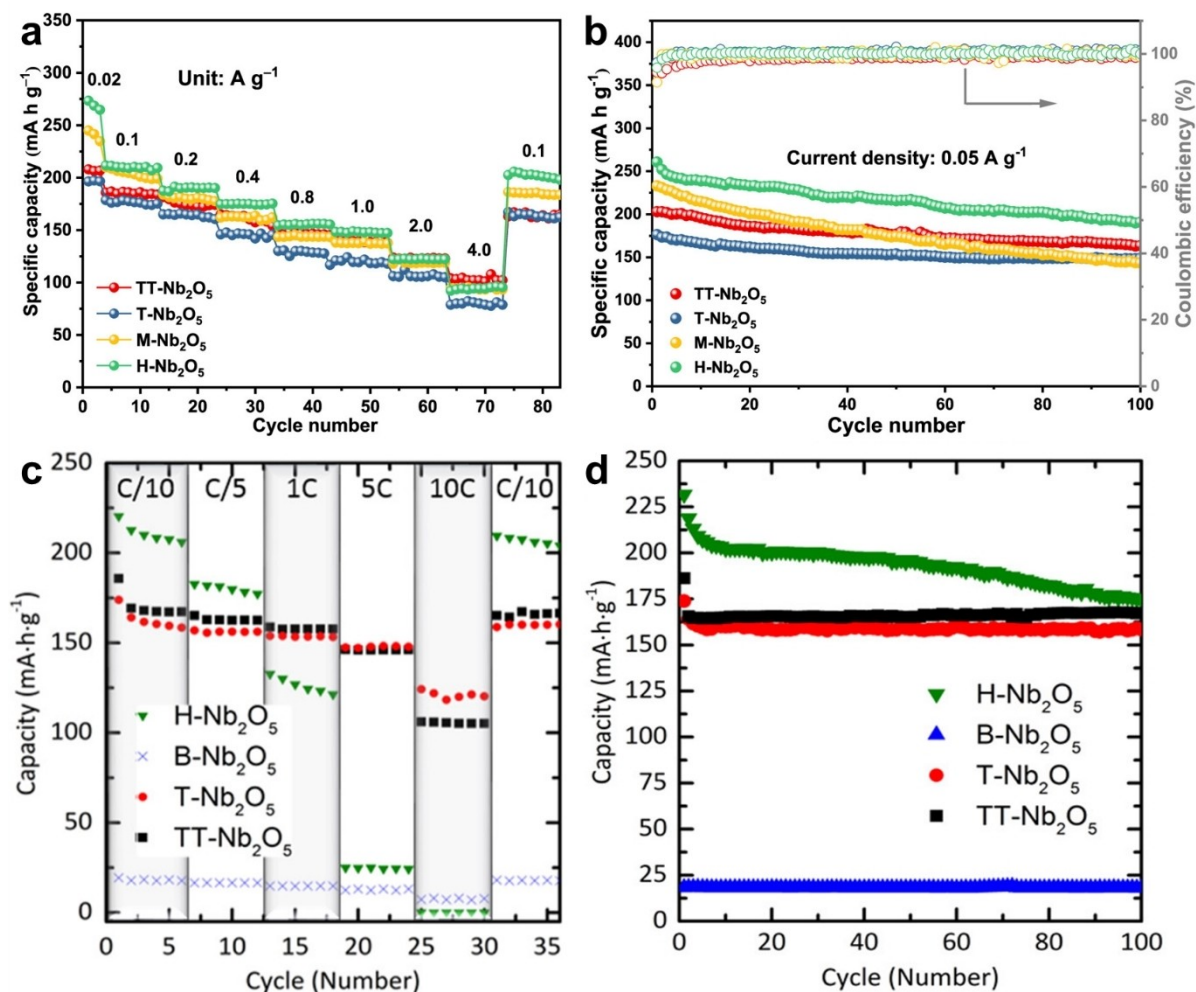
ChemElectroChem

Review

doi.org/10.1002/celc.202300581

Chemistry
Europe

European Chemical
Societies Publishing

Figure 3. Rate performances of Nb_2O_5 polymorphs tested (a) at different current densities from 0.02 to 4.0 $A\,g^{-1}$ between 1.0 and 3.0 V (c) at C/10–10 C between 1.2 and 3.0 V. (b) Cycling stabilities and Coulombic efficiencies of Nb_2O_5 polymorphs tested at the current density of 0.05 $A\,g^{-1}$. Reproduced from Ref. [27]. Copyright (2021), with permissions from American Chemical Society. (d) Cycling stabilities at either 1 C (T, TT) or C/10 (B, H) with a constant voltage charge step. Reproduced from Ref. [28]. Copyright (2016), with permissions from American Chemical Society.

3.1. Electron microscopy

Scanning electron microscopy (SEM) and transmission electron microscopy (TEM) are the most commonly used electron microscopy methods to study the morphology of battery materials.

Li et al.[47] developed orthorhombic Nb_2O_5 nanotubes by atomic layer deposition methods using polyacrylonitrile nanofibers as a sacrificing template. Figure 5a shows the Field Emission SEM images of Nb_2O_5 nanotubes, from which the hollow nanotube structure can be seen. The unique structure could provide fast Li diffusion kinetics. Energy-dispersive X-ray Spectrometry (EDS or EDX) is usually used in conjunction with electron microscopy to provide the elemental composition and distribution of the sample. Figure 5b–d shows the EDX mapping results of the distribution of Nb and O elements in the Nb_2O_5 nanotube.

TEM can provide not only morphological information but crystal structural information, depending on the operation modes used to investigate the sample. Figure 5e shows the TEM image of T–Nb_2O_5 which provides the thickness information of nanotubes. Figure 5f shows a high-resolution TEM (HRTEM) image and the corresponding fast Fourier transform (FFT) patterns (inset of Figure 5) of T–Nb_2O_5, which provides the d-spacing information and its corresponding lattice planes.

Andoni et al.[48] used ex situ TEM to analyse the degradation of T–Nb_2O_5 films by cycling the electrodes up to 10000 cycles. The disordered and deformation of crystallinity could be seen in the marked planes at 1, 1000 and 2000 cycles. At first lithiation cycle, the doubling of the reflections indicates the incomplete lithiation while the first delithiation cycle retains its orthorhombic structure. At 1000 cycles the sample shows disordered and deformed structure in its lithiated and delithiated states, respectively. After 2000 cycles, the crystal structure is severely distorted which leads to the degradation of the electrode.
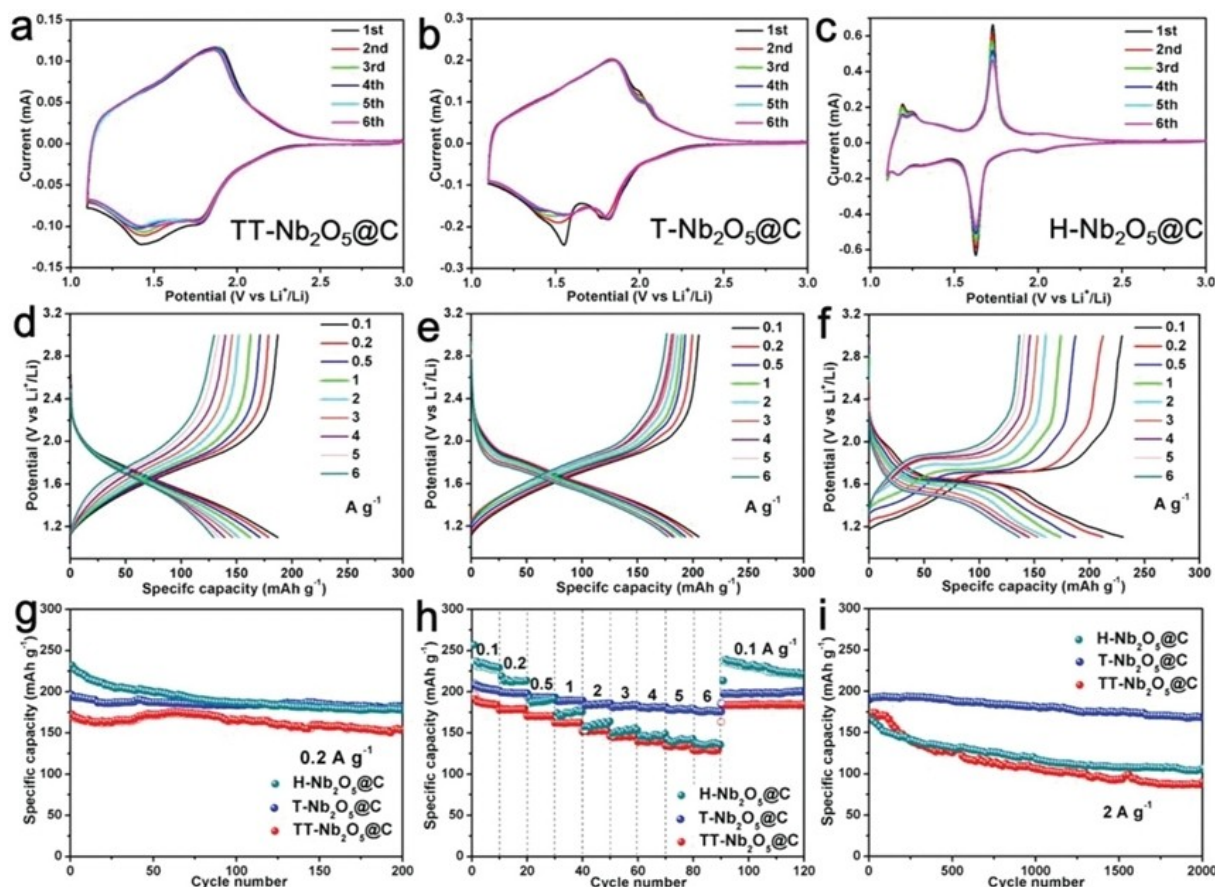
Figure 4. The electrochemical performance of three carbon-confined Nb_2O_5 samples, $TT–Nb_2O_5@C$, $T–Nb_2O_5@C$, and $H–Nb_2O_5@C$. (a-c) The first six CV curves tested at a scan rate of 0.2 mV s^{-1}. (d–f) Charge–discharge curves at different current densities. (g) Cycling performances tested at a low current density of 0.2 A g^{-1}. (h) Rate performances tested at various current densities ranging from 0.1, 0.2, 0.5, 1, 2, 3, 4, 5, and 6, back to 0.1 A g^{-1}. (i) Cycling performances tested at a high current density of 2 A g^{-1}. Reproduced from Ref. [36]. Copyright (2019), with permissions from Wiley.

3.2. X-ray Computed Tomography (CT)

Focused ion beam (FIB) SEM and X-ray micro- and nano-computed tomography are widely used 3D imaging techniques in Li ion battery research. The spatial resolution of FIB-SEM could reach down to ca. 10 nm while the technique physically removes the surface of the sample layer by layer after images of each layer are collected, which makes it unsuitable for *in situ* or *operando* studies on Li-ion battery electrodes.[50,51] X-ray computed tomography, on the other hand, is a non-destructive imaging technique which combines X-ray imaging and computer processing to obtain a three-dimensional image of a sample. Traditional CT is used frequently for medical purposes, but in recent years lab-based or synchrotron CT has found application in a range of materials science domains including the investigation of battery electrodes at multiple length and time scales.[52–55] Lin et al.[49] first used CT to investigate the macroscopic 3D morphology of commercial Nb_2O_5 material. Commonly studied parameters for Li ion battery electrodes, such as particle size, porosity and tortuosity, are important metrics of morphology and critical for understanding of the ionic diffusivity of electrolytes in electrode.[56] Moreover, the spatial information of particle size and shape factor could be

visualized from the CT results, which could provide unique information on 3D morphology of electrode for battery materials. These results could be used as the basis for further image-based modelling work to parameterize the solid-state diffusion coefficient and exchange current density of Nb_2O_5.

3.3. X-ray diffraction (XRD)

X-ray Diffraction (XRD) is a widely-adopted technique to investigate the structural information of crystalline materials, from which the information of crystal phase, *d*-spacing, unit-cell size and crystallinity can be obtained. For lithium ion battery (LIB) research, it is important to understand the changes to the electrode phases, lattice parameters and volume expansion/contraction during charge and discharge process to reveal the charge storage mechanisms and degradation mechanisms of electrodes.[57] Thus, it is valuable to carry out both lab-based or synchrotron-based *ex situ, in situ* and *operando* XRD study to investigate the battery materials.

Due to the many different phases of Nb_2O_5 material possible, XRD is a critical characterisation step for new material synthesis covering how researchers demonstrate phase purity

ChemElectroChem

Review
doi.org/10.1002/celc.202300581

Chemistry Europe
European Chemical
Societies Publishing

Table 2. The electrochemical performance of different Nb_2O_5 polymorphs for lithium-ion batteries.

Material	Capacity mAh g^{-1}	Rate capability mAh g^{-1}	Voltage range V vs. Li$^+$/Li	Ref
TT–Nb_2O_5	207@0.1 C	103@20 C	1.0–3.0	[27]
TT–Nb_2O_5	168@0.1 C	106@10 C	1.2–3.0	[28]
TT–Nb_2O_5	139@0.25 C	58@10 C	1.0–3.0	[37]
TT–Nb_2O_5@C	187@0.5 C	129@30 C	1.1–3.0	[36]
TT–Nb_2O_5	191@0.25 C	114@5 C	1.2–3.0	[38]
TT–Nb_2O_5	183@0.2 C	85@20 C	1.0–3.0	[39]
T–Nb_2O_5	197@0.1 C	80@20 C	1.0–3.0	[27]
T–Nb_2O_5	160@0.1 C	8@60 C	1.2–3.0	[28]
T–Nb_2O_5	154@0.25 C	85@10 C	1.0–3.0	[37]
T–Nb_2O_5@C	205@0.5 C	177@30 C	1.1–3.0	[36]
T–Nb_2O_5	224@0.2 C	79@25 C	1.1–3.0	[40]
Bl T–Nb_2O_5 nanorods	248@0.2 C	121@25 C	1.1–3.0	[40]
T–Nb_2O_5	152@0.25 C	80@5 C	1.2–3.0	[38]
T–Nb_2O_5 nanobelt	205@0.5 C	54@50 C	1.2–3.0	[41]
T–Nb_2O_5	152@1 C	115@10 C	1.0–3.0	[42]
T–Nb_2O_5/graphene	60@1.25 C	26@10 C	0.8–3.0	[43]
T–Nb_2O_5	216@0.25 C	38@25 C	1.0–2.6	[44]
T–Nb_2O_5 nanofibers	193@0.25 C	70@25 C	1.0–2.6	[44]
B–Nb_2O_5	18@0.1 C	8@10 C	1.2–3.0	[28]
M–Nb_2O_5	240@0.1 C	94@20 C	1.0–3.0	[27]
M–Nb_2O_5	170@0.25 C	141@10 C	1.0–3.0	[37]
H–Nb_2O_5	269@0.1 C	94@20 C	1.0–3.0	[27]
H–Nb_2O_5	208@0.1 C	25@5 C	1.2–3.0	[28]
H–Nb_2O_5	164@0.25 C	125@10 C	1.0–3.0	[37]
H–Nb_2O_5 nanowire	198@0.1 C	139@2.5 C	1.2–3.0	[45]
H–Nb_2O_5@C	231@0.5 C	137@30 C	1.1–3.0	[36]
RS–Nb_2O_5	269@0.1 C	191@5 C	0.5–3.0	[46]
amorphous	180@0.1 C	73@5 C	0.5–3.0	[46]
amorphous	149@0.25 C	47@5 C	1.2–3.0	[38]

Table 3. List of common characterisation techniques to study Nb_2O_5 material in LIBs.

Technique	Information provided			Capabilities
	Morphology	Structure	Chemistry	
SEM	√			Provide morphology information with a nm scale resolution
TEM	√	√		Provide ultrahigh resolution images and structural information
EDS	√		√	Provide elemental distribution and quantitative information
XCT	√			3D morphology information with a resolution from nm scale to μm scale without damage
XRD		√		Provide the structural information of crystalline materials
XPS			√	Measure oxidation state of element and provide semi-quantitative information
XAS		√	√	Provide oxidation state, coordination, and structural information
Raman		√	√	Provide structural information of chemical species
NMR		√	√	Provide electronic and structural information of samples

of materials prepared at various conditions. Griffith et al.[28] carefully prepared different phases of Nb_2O_5 from annealing of NbO_2 at temperatures between 200 °C to 1100 °C for 24 h with a temperature step of 50 °C. The XRD patterns of NbO_2, TT–, T–, B– and H–Nb_2O_5 are shown in Figure 6a. The XRD result shows that the TT- Nb_2O_5 is formed at 300 °C and T- Nb_2O_5 is formed at

ChemElectroChem

Review
doi.org/10.1002/celc.202300581
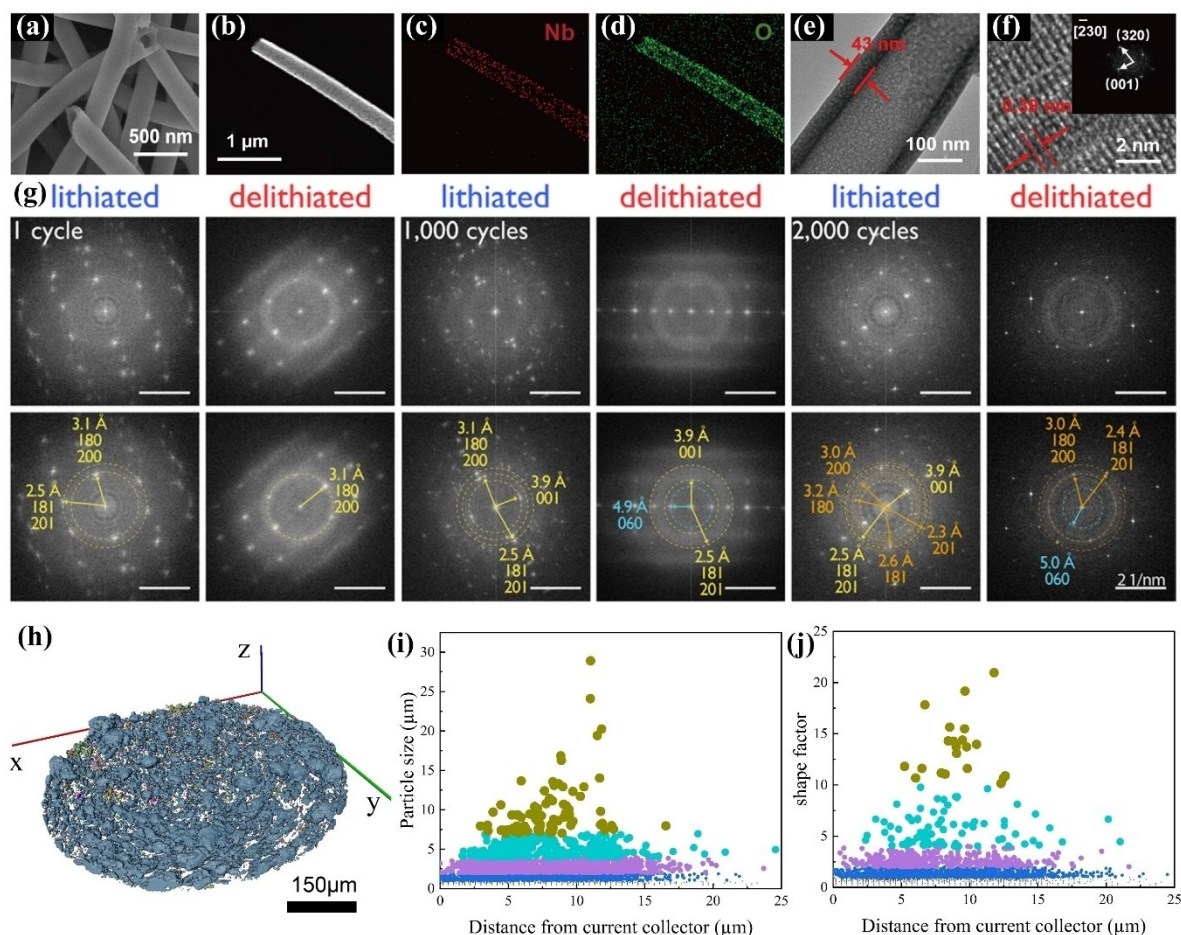
Chemistry
Europe
European Chemical
Societies Publishing

Figure 5. (a) Field-emission SEM image of T–Nb$_2$O$_5$ nanotubes. (b-d) EDS images of T–Nb$_2$O$_5$ nanotubes. (e) High resolution TEM images of T–Nb$_2$O$_5$ nanotubes and (f) corresponding FFT pattern. Reproduced from Ref. [47]. Copyright (2021), with permissions from American Chemical Society. (g) Raw FFTs of atomic resolution TEM images (top) are paired with assignments (bottom) for lithiated and delithiated films at 1, 1000, and 2000 cycles. Reproduced from Ref. [48]. Copyright (2021), with permissions from American Chemical Society. (h) Reconstructed CT image of commercial Nb$_2$O$_5$ electrode. Spatial distribution of (i) particle sizes and (j) shape factor of commercial Nb$_2$O$_5$ electrode. Reproduced from Ref. [49]. Copyright (2023), with permissions from Elsevier.

550 °C. The material annealed between 450 °C to 500 °C shows a mixture of TT– and T–Nb$_2$O$_5$. When further increasing the annealing temperature to 700 °C, the B–Nb$_2$O$_5$ is formed and the H–Nb$_2$O$_5$ is formed above 900 °C.

More detailed information about the way the materials behave can be garnered from *in situ* or *operando* XRD, which allows for the study of the evolution of crystallography with state of lithiation under different cycling conditions such as temperature, C-rate or long cycles. Wu et al.[58] carried out an *in situ* XRD study on T–Nb$_2$O$_5$ supported on N-doped carbon electrode to investigate the lithium storage process (Figure 6b). Their results showed that three diffraction peaks shifted to lower angles during the discharge process of T–Nb$_2$O$_5$, which indicated the expansion of its lattice spacing during lithiation. The peaks then return to their original 2θ degree in the delithiation process. The XRD patterns showed a good reversibility in the first 5 cycles.

It is worth noting that in future work, the relationship between the capacity fade and the electrochemical energy storage mechanisms of the batteries can be studied by *operando* XRD to further understand the degradation process of

electrodes. Compared to laboratory XRD, synchrotron facilities have advantages of better photon flux, penetration depth and brightness, which can acquire XRD pattern within the scale of milliseconds, therefore making it particularly well suited to studying the lithiation behaviour of these materials at high C-rates, and the potential contributions to capacitive and lithiation storage seen in previous electrochemical work.[49,58]

3.4. X-ray photoelectron spectroscopy (XPS)

X-ray photoelectron spectroscopy is a powerful technique to analyse the oxidation states and elemental composition of the surface of the materials. When combined with the depth profile function, it can provide internal elemental composition and valence bond information. It is worth noting that the sample preparation for XPS could be of great importance to get accurate results because the oxidation states of surface elements could be oxidized if the sample is not properly preserved.
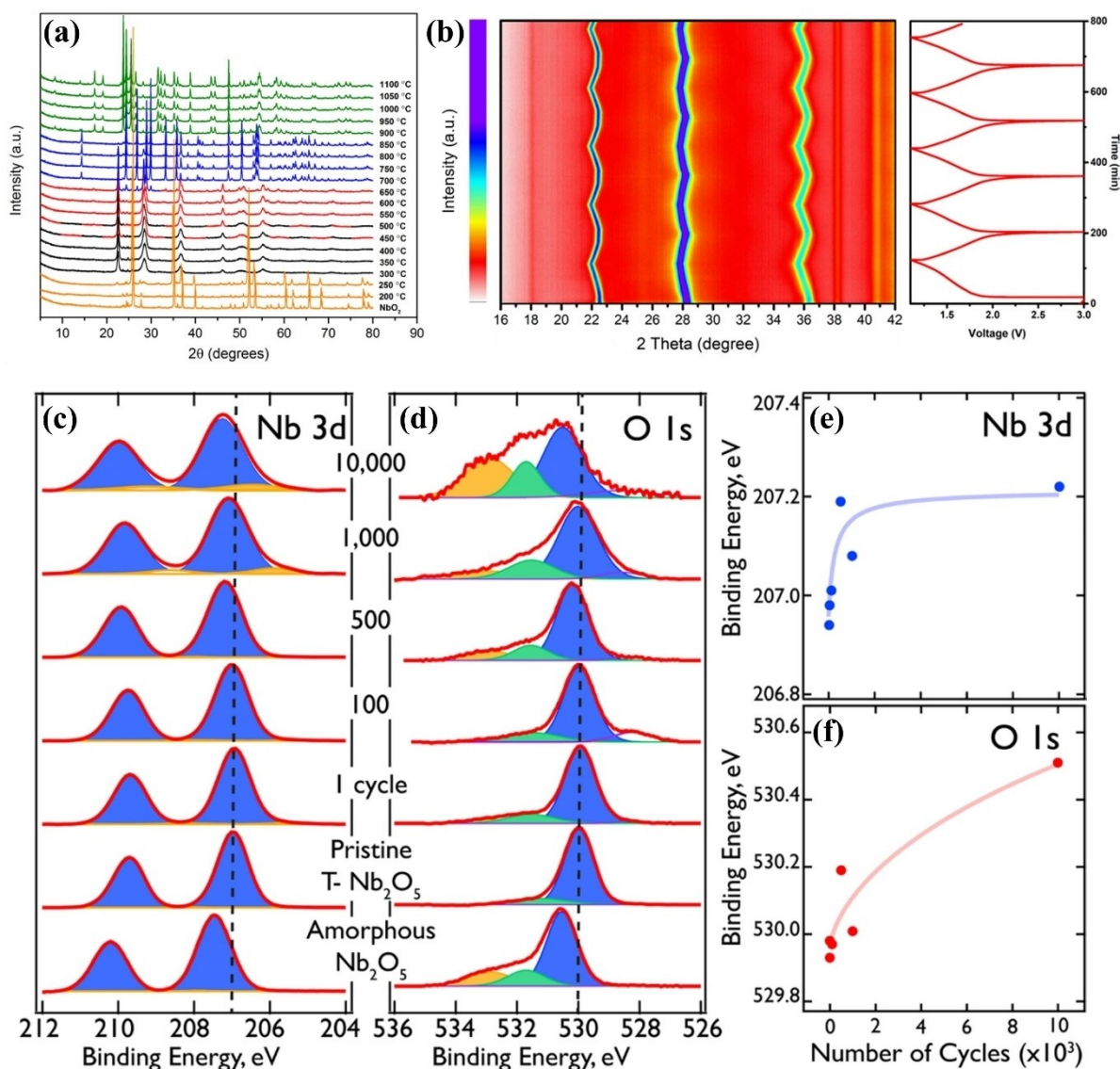
ChemElectroChem

Review
doi.org/10.1002/celc.202300581

Chemistry Europe
European Chemical
Societies Publishing

Figure 6. (a) XRD patterns of phases observed upon heating NbO_2 in air. The patterns dominated by NbO_2, $TT–Nb_2O_5$, $T–Nb_2O_5$, $B–Nb_2O_5$, and $H–Nb_2O_5$ are shown in orange, black, red, blue, and green, respectively. Reproduced from Ref. [28]. Copyright (2016), with permissions from American Chemical Society. (b) *In situ* XRD patterns of Nb_2O_5@NC samples during galvanostatic charge and discharge at $0.2\ Ag^{-1}$. (c–f) XPS analysis of delithiated $T–Nb_2O_5$ as a function of the number of lithiation/delithiation cycles. Reproduced from Ref. [58] Copyright (2016), with permissions from American Chemical Society. In (c), blue fittings correspond to Nb^{5+}, and orange corresponds to Nb^{4+}. In (d), blue corresponds to lattice O^{2-}, green corresponds to non-lattice oxygen, and orange corresponds to adsorbed OH^- and H_2O. (e) Plot of Nb 3d binding energy vs number of cycles, (f) plot of O 1s binding energy vs number of cycles. Reproduced from Ref. [48]. Copyright (2021), with permissions from American Chemical Society.

Andoni et al.[48] tracked the changes of elements by *ex situ* XPS experiment on $T–Nb_2O_5$ for 10000 cycles. The XPS results showed Nb 3d and O 1s peaks shifted to higher binding energies with the cycling of electrodes. Both of Nb 3d and O 1s peaks were found to broaden after cycling, which indicated that $T–Nb_2O_5$ could become more amorphous after cycling.

3.5. X-ray absorption spectroscopy (XAS)

X-ray absorption spectroscopy is an insightful technique to investigate the electronic and structural properties of the material. XAS is an element-specific technique, using X-rays

with energies around the absorption edge of interest for a particular element. It is usually carried out in synchrotron facilities due to the requirement for high energy resolution, tuneable monochromic X-rays to provide high-quality XAS spectra, although lab XAS systems are becoming increasingly common;[59] synchrotron techniques have the benefit of high X-ray flux allowing for time-resolved *operando* experiments and realistic *in situ* environments. XAS includes X-ray absorption near-edge structure (XANES) and extended X-ray absorption fine structure (EXAFS). XANES spectra can provide information about oxidation states and coordination environment, while EXAFS spectra provide insights into the bond distance, bond angle and coordination numbers of neighbouring atoms.

ChemElectroChem

Review

doi.org/10.1002/celc.202300581

Chemistry
Europe
European Chemical
Societies Publishing

Li et al.[60] carried out *operando* Nb K-edge XAS experiments on T–Nb$_2$O$_5$ and H–Nb$_2$O$_5$ to study the electronic and structural change of the material. The XANES results (Figure 7a,b) showed that the absorption edge of both T–Nb$_2$O$_5$ and H–Nb$_2$O$_5$ shifts to lower energy during lithiation as Nb^{5+} atoms were reduced in this process. However, the H–Nb$_2$O$_5$ showed wider variation range than T–Nb$_2$O$_5$. In the delithiation process, T–Nb$_2$O$_5$ had a negative shift compared to pristine material which led to a lower Columbic efficiency, while H–Nb$_2$O$_5$ had a better reversibility than T–Nb$_2$O$_5$ as the absorption edge could fully overlap with its pristine spectra after cycling.

The local structure and coordination environment was further studied by *operando* EXAFS (Figure 7c,d). In the pristine state, the oxygen in the dense-packed 4 h atomic layer had a larger shielding effect on Nb–Nb scattering of T–Nb$_2$O$_5$ than H–Nb$_2$O$_5$. In the lithiation process, Nb–O peaks of both T- and H–Nb$_2$O$_5$ increased, which could be a result of alleviating of Jahn-Teller effect with the intercalation of Li ions. The Nb–Nb peak decreased for H–Nb$_2$O$_5$ during lithiation process due to the shielding effect caused by the insertion of Li ions. After one

cycle, the Nb–Nb peak of T–Nb$_2$O$_5$ almost disappeared, which means that Li ions may remain in the interlayer.

It is worth noting that although synchrotron XAS is a powerful tool to study batteries, the X-ray beam damage on samples is not negligible for *operando* study of batteries, which requires researchers to use this powerful technique carefully and cleverly to limit or avoid the beam damage on samples.[61] Due to the high C-rate properties of Nb$_2$O$_5$ materials, it would be interesting to see more research conducted under high C-rate and controlled temperature conditions in this research field.

3.6. Raman spectroscopy

Raman spectroscopy is a simple and useful technique to obtain information, such as molecular structure, molecular composition and chemical bonding, by analysing the vibrational and rotational modes of molecules. However, the broad bandwidths and irregular band profiles of T–Nb$_2$O$_5$, which could be caused by the overlapping of more than 150 independent vibrational
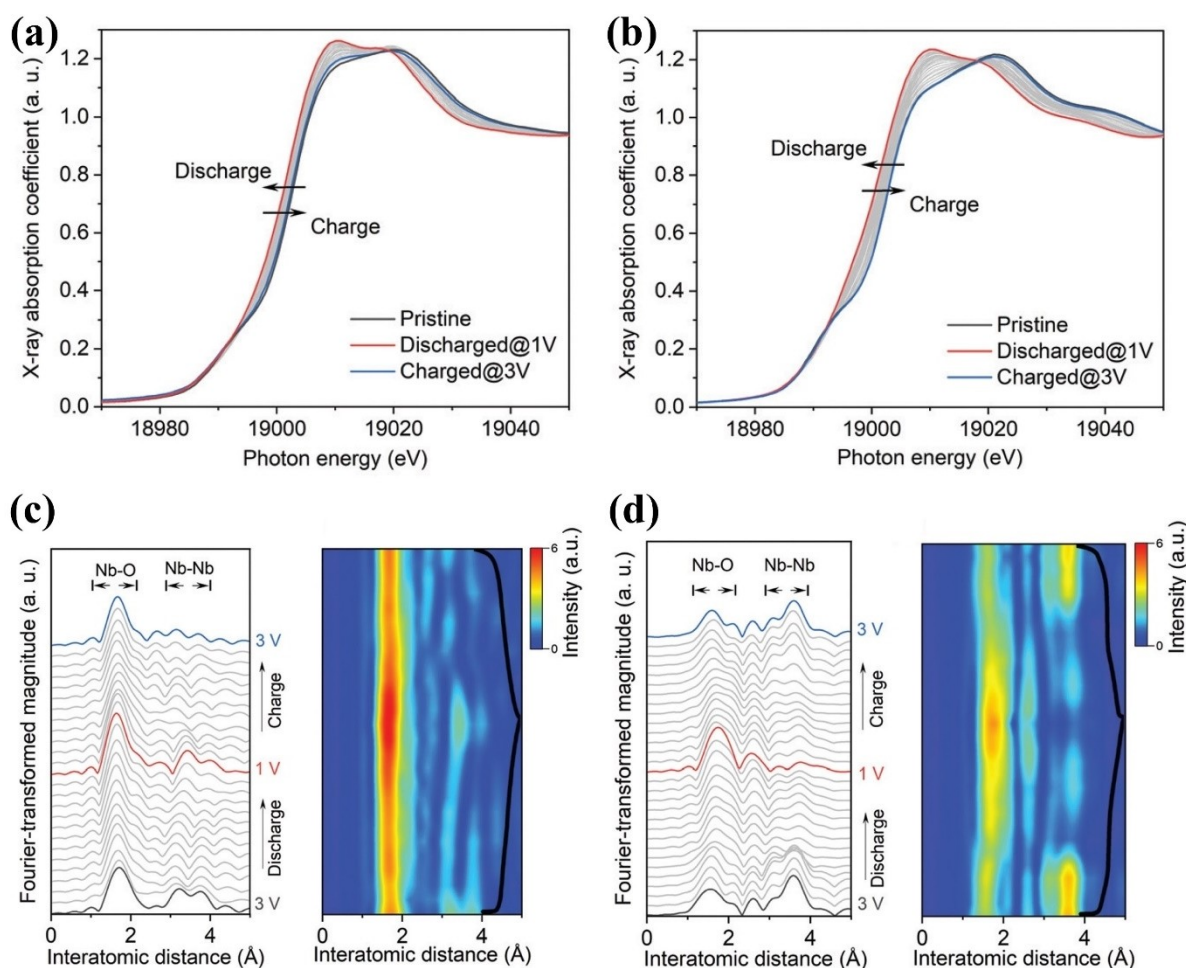

Figure 7. *Operando* Nb K-edge X-ray absorption near edge structure (XANES) profiles for (a) T–Nb$_2$O$_5$ and (b) d-H–Nb$_2$O$_5$ at 0.25 C. Radial distribution function (RDF) of Nb K-edges *operando* EXAFS spectra and their corresponding 2D contour plot for the electrode of (c) T–Nb$_2$O$_5$ and (d) d-H–Nb$_2$O$_5$ at 0.25 C. The electrochemical discharge/charge profile (black curve) of *operando* cell was overlaid in the right side of contour plot. Reproduced from Ref. [60]. Copyright (2022), with permissions from Royal Society of Chemistry.

ChemElectroChem

Review
doi.org/10.1002/celc.202300581

**Chemistry
Europe**
European Chemical
Societies Publishing

modes of T–Nb_2O_5, make the Raman spectrum hard to deconvolute for individual peaks, and subsequently difficult to interpret. Chen et al.[62] combined *operando* Raman spectroscopy with a computational study to unveil the charge-transfer mechanisms of Li ions in T–Nb_2O_5. Figure 8a shows the reversibility of Raman spectroscopic evolution for nine cycles. The intensity of three areas of ν periodically increased and decreased, which indicates the reversibility of structure evolution induced by the lithiation and delithiation processes. The Raman spectra in Figure 8b further indicates that the ν_{hi}, ν_{mid} and ν_{low} signal will decrease to zero, split gradually and experience a minor blue shift, respectively, during the lithiation

process. In combination with computational modelling, the results showed that Li ion will locate at the loosely packed 4 g layers and bridge with oxygens in 4 h layers, which will form unique paths for low-hindrance diffusion of Li ions.

3.7. Nuclear Magnetic Resonance (NMR)

Nuclear Magnetic Resonance spectroscopy is a powerful characterisation method to study the chemical environments by measuring the absorption of electromagnetic radiations of samples in a static magnetic field.
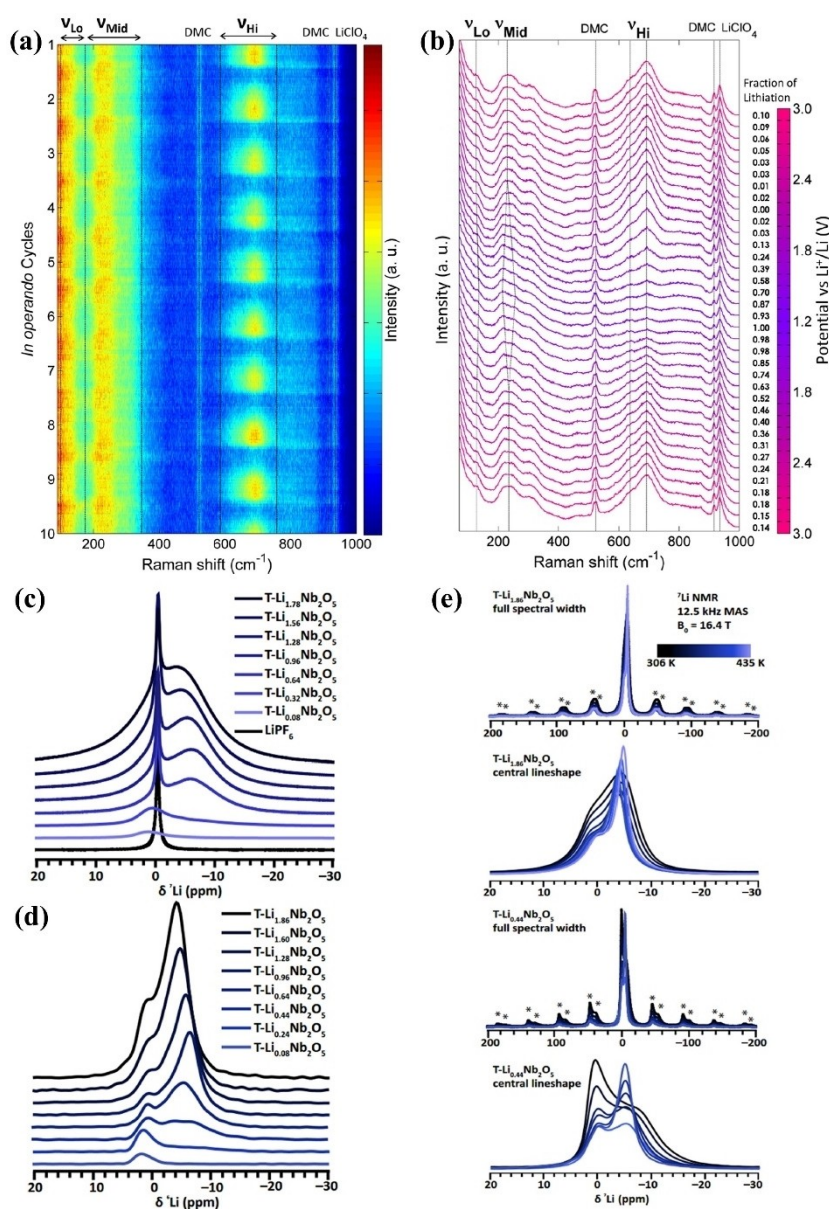

Figure 8. (a) *In operando* Raman spectroscopic evolution of a T–Nb_2O_5 thin-film electrode acquired in 9 cycles. In each cycle, the electrochemical potential is cycled from 3.0 to 1.2 V and back to 3.0 V. Major Raman band groups of T–Nb_2O_5 and electrolyte bands are marked. (b) *In operando* Raman spectroscopic evolution of a T–Nb_2O_5 thin-film electrode as its potential was varied from 3 V to 1.2 V and to 3 V (vs Li⁺/Li). Reproduced from Ref. [62]. Copyright (2017), with permissions from American Chemical Society. (c) ⁷Li MAS NMR of $Li_xNb_2O_5$ spectra at 9 kHz MAS and 4.7 T, and (d) ⁶Li MAS NMR of $Li_xNb_2O_5$ spectra at 9 kHz MAS and 16.4 T. (e) Variable-temperature ⁷Li MAS NMR of $Li_xNb_2O_5$ at 12.5 kHz at 16.4 T. Reproduced [28]. Copyright (2016), with permissions from American Chemical Society.

ChemElectroChem

Review
doi.org/10.1002/celc.202300581

**Chemistry
Europe**
European Chemical
Societies Publishing

Griffith et al.[28] used ^{6}Li and ^{7}Li magic angle spinning (MAS) NMR to investigate the lithium dynamics in the lithiation process of $T–Nb_2O_5$. The sharp peak in Figure 8c is from the residual $LiPF_6$ and the small peak is from the intercalation of lithium. In Figure 8d, the peak at 2 ppm is from the occupation of first lithium ions, while the peak at around −5 ppm increases with the state of lithiation above $Li_{0.2}Nb_2O_5$. Variable-temperature ^{7}Li MAS NMR experiments were carried out to study the time scales for lithium motion and the electronic structure of the electrodes. The results demonstrated the effect of temperature on the shape and shift of ^{7}Li in $Li_{0.44}Nb_2O_5$ and $Li_{1.86}Nb_2O_5$, revealing the occurrence of electron delocalization through the Nb–O–Nb network in $T–Nb_2O_5$ during lithiation. The chemical shifts at high Li-ion intercalation state indicates delocalized conduction electrons and clarify the electronic aspect of the observed high-rate performance in this originally wide-bandgap oxide.

4. Summary and Outlook

Nb_2O_5 is an emerging anode material for lithium-ion batteries. Despite the theoretical capacity (202 mAh g^{-1}) of Nb_2O_5 being lower than that of the commercial graphite anode (372 mAh g^{-1}), their great rate performance is attractive to many high-power applications, which allow them to be cycled at 10–100 C while still delivering reasonable charge capacity. As the normal operating voltage window of Nb_2O_5 is above 1.0 vs. Li/Li$^+$, it can mitigate common issues of SEI formation and dendrite growth that are critical in the graphite anode and account for battery ageing and short circuit. On the other hand, Nb_2O_5 possesses diverse crystal structures and forms a large family of many different polymorphs, which have exhibited large variations in electrochemical properties, charge capacity, rate capability, and cycling stability. Typical Nb_2O_5 polymorphs that are suitable for battery applications include $TT–$, $T–$, $M–$, and $H–Nb_2O_5$.

Using a wide range of structural, elemental, and electrochemical characterisation techniques, the unique behaviours and performances of different Nb_2O_5 can be probed, observed, investigated, and attributed to their characteristic structures and properties. For example, two key charge storage mechanisms are discovered and show varying contributions to the electrochemical performance of different Nb_2O_5 polymorphs. The orthorhombic structure of $T–Nb_2O_5$ and its disordered phase of $TT–Nb_2O_5$ allow fast 2D Li diffusion and intercalation into their crystal structure, yielding their distinct feature of intercalation pseudocapacitance which exhibits strong capacitive effect particularly at high C-rates and enables ultrafast (dis)charging. In contrast, the crystal structures of tetragonal $M–Nb_2O_5$ and monoclinic $H–Nb_2O_5$ limit Li diffusion, which lowers their rate performance but supports higher charge capacity.

Compared to many other transition metal oxides (e.g., $LiCoO_2$, $LiMn_2O_4$), there is a current lack of understanding of several important characteristics of Nb_2O_5, such as physical properties (e.g., effective electrical and ionic conductivities),

spatial crack formation information, heat generation, and thermal runaway under different C-rate conditions. Owing to the high-rate capability of Nb_2O_5, the electrochemical processes observed at low C-rates may not be consistent with those taking place at high C-rates. The ageing mechanisms of Nb_2O_5 are crucial for its future improvement, scale-up and commercialization in LIBs, but have remained as mysteries with scarce characterisations beyond 100 cycles. All of these require more comprehensive investigations of the rate dependence of electrochemical processes and the electrochemical-thermal-mechanical coupling in Nb_2O_5.

As cracking studies, *operando* cracking of $Nb_{14}W_3O_{44}$ anode material has been observed using optical scattering microscopy on dilute electrodes, providing a 2D view of crack initiation and propagation perpendicular to the lithiation direction, which illustrated the cracking of particle was caused by SOC heterogeneities.[63] Similar methods could be used to compare the cracking mechanisms in Nb_2O_5, albeit providing information in only the 2D plane. Furthermore, lab-based micro-CT and nano-CT are suitable techniques to carry out non-destructive 3D tomography investigation on pristine and aged electrodes with a maximum spatial resolution of tens of nm. Alternatively, FIB-SEM can also achieve high resolution 3D tomograms, but this is a destructive technique and may only be suitable for *ex situ* study on batteries. Additionally, the tomography data could be used as a base for further modelling work to study the influence of cracking particles on electrolyte diffusivity, as in other Li-ion battery materials.[64–66] Moreover, synchrotron X-ray CT, which has better temporal resolution compared to lab-based CT, allows researchers to do *in situ/operando* tomography study on battery cells to understand when and under which experiment conditions the crack happens. Due to the complex relationship between the formation of crack and battery performance, it is hard to correlate the performance with cracking to explain the degradation of batteries. However, *operando* degradation study can be carried out by synchrotron CT to possibly explain the performance decay caused by cracking.

Due to the high C-rate capability of Nb_2O_5 material, it is worth carrying out *operando* studies by various techniques to monitor the energy storage behaviour under different C-rate conditions. As for *operando* XRD study, currently laboratory XRD is widely used due to its availability, ease of access and affordability. However, laboratory XRD usually takes several minutes to acquire one pattern, which is not suitable for *operando* XRD study under high C-rate. In this case, researchers can make use of the powerful synchrotron XRD facility with the capability of acquiring patterns in fractions of seconds through *operando* cell housings, such as ID11 beamline at ESRF (France), which makes it possible to understand the electrochemical behaviour under high C-rate by *operando* XRD studies. Moreover, *operando* XRD can investigate the energy storage mechanisms of batteries such as solid solution mechanism, two-phase mechanism or a combination of solid solution and phase transfer mechanism by studying the shift and appearance of characteristic peaks of material. Additionally, fatigue peaks may also appear in the degradation process of electrode, which can

ChemElectroChem

Review

doi.org/10.1002/celc.202300581

**Chemistry
Europe**
European Chemical
Societies Publishing

further illustrate the relationship between electrochemical performance decay and changes in the material. For *operando* XAS study in synchrotron facilities, a few beamlines such as BL01B1 (SPring-8, Japan), are capable of acquiring XAFS spectra with time resolution of around 10 s, which makes *operando* study for high C-rate battery study possible. *Operando* XAS results can illustrate the changes of oxidation states of materials during different C-rate at various charging/discharging states, which leads to the understanding of capacitance retention under different conditions.[60] Furthermore, the behaviour of batteries undergone significant ageing can also be studied by coupling the XAS results with the electrochemical results.

Despite multiple cutting-edge techniques having been applied to studying Nb_2O_5, different characterisation methods require various customised *in situ* or *operando* cells to carry out the battery testing. However, most of the existing or commercial cells do not support the control of temperature and applied pressure, let alone high-current cycling. To meet the requirements for the challenging Nb_2O_5 characterisations, more technologically relevant cell designs have to be developed and adapted to the testing and characterisation systems. It is also worth noting that as well as the fundamental rate/lithiation properties of the materials/particles themselves, electrode formulation, mixing sequences in slurry preparation and electrode design are key factors in the electrochemical performance of electrodes and worth studying in the future work on Nb_2O_5 anode materials.[67,68]

Acknowledgements

Conflict of Interests

The authors declare no conflict of interest.

Keywords: Anode · Characterisation · Fast charging · Lithium-ion batteries · Niobium pentoxide

[1] T. M. Gür, *Energy Environ. Sci.* **2018**, *11*, 2696–767.
[2] S. Chu, Y. Cui, N. Liu, *Nat. Mater.* **2016**, *16*, 16–22.
[3] J. Li, Z. Li, S. Tang, J. Hao, T. Wang, C. Wang, L. Pan, *Carbon* **2023**, *203*, 469–78.
[4] D. Wang, Q. Li, Y. Zhao, H. Hong, H. Li, Z. Huang, G. Liang, Q. Yang, C. Zhi, *Adv. Energy Mater.* **2022**, *12*, 2102707.
[5] J. Xie, X. Li, H. Lai, Z. Zhao, J. Li, W. Zhang, W. Xie, Y. Liu, W. Mai, *Angew. Chem. Int. Ed.* **2019**, *58*, 14740–7.
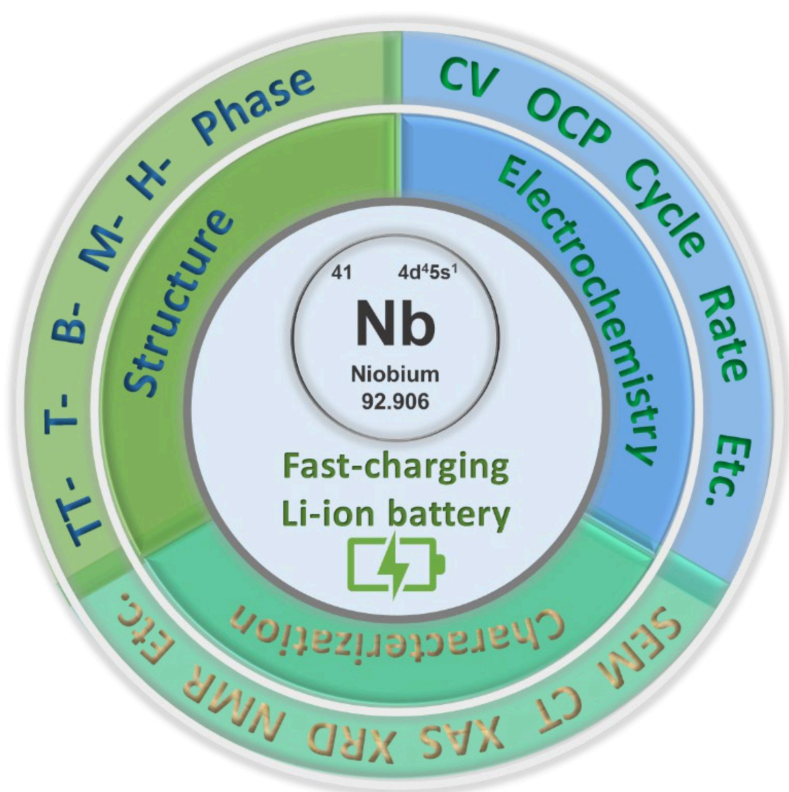[6] B. C. Gibb, *Nat. Chem.* **2021**, *13*, 107–9.
[7] G. Zubi, R. Dufo-López, M. Carvalho, G. Pasaoglu, *Renewable Sustainable Energy Rev.* **2018**, *89*, 292–308.
[8] Y. Zhang, C.-Y. Wang, X. Tang, *J. Power Sources* **2011**, *196*, 1513–20.
[9] P. P. Paul, V. Thampy, C. Cao, H.-G. Steinrück, T. R. Tanim, A. R. Dunlop, E. J. Dufek, S. E. Trask, A. N. Jansen, M. F. Toney, J. Nelson Weker, *Energy Environ. Sci.* **2021**, *14*, 4979–88.
[10] I. Zilberman, S. Ludwig, M. Schiller, A. Jossen, *J. Energy Storage* **2020**, *28*, 101170.
[11] Q. Deng, Y. Fu, C. Zhu, Y. Yu, *Small* **2019**, *15*, e1804884.
[12] F. Xie, J. Xu, Q. Liao, Q. Zhang, B. Liu, L. Shao, J. Cai, X. Shi, Z. Sun, C.-P. Wong, *Energy Reviews* **2023**, *2*, 100027.
[13] N. A. Dsouki, M. P. de Lima, R. Corazzini, T. M. Gáscon, L. A. Azzalis, V. B. C. Junqueira, D. Feder, F. L. A. Fonseca, *J. Mater. Sci. Mater. Med.* **2014**, *25*, 1301–5.
[14] C. Nico, T. Monteiro, M. P. F. Graça, *Prog. Mater. Sci.* **2016**, *80*, 1–37.
[15] H. Ding, Z. Song, H. Zhang, H. Zhang, X. Li, *Mater. Today Nano* **2020**, *11*, 100082.
[16] H. Schäfer, R. Gruehn, F. Schulte, *Angew. Chem. Int. Ed.* **1966**, *5*, 40–52.
[17] K. Kato, S. Tamura, *Acta Crystallogr. Sect. B* **1975**, *31*, 673–7.
[18] N. Kumagai, Y. Koishikawa, S. Komaba, N. Koshiba, *J. Electrochem. Soc.* **1999**, *146*, 3203.
[19] F. Shen, Z. Sun, Q. He, J. Sun, R. B. Kaner, Y. Shao, *Mater. Horiz.* **2021**, *8*, 1130–52.
[20] H. Park, D. Lee, T. Song, *J. Power Sources* **2019**, *414*, 377–82.
[21] L. Frevel, H. Rinn, *Anal. Chem.* **1955**, *27*, 1329–30.
[22] S. Pérez-Walton, C. Valencia-Balvín, G. M. Dalpian, J. M. Osorio-Guillén, *physica status solidi (b)* **2013**, *250*, 1644–50.
[23] T. S. Ercit, *Mineral. Petrol.* **1991**, *43*, 217–23.
[24] W. Mertin, S. Andersson, R. Gruehn, *J. Solid State Chem.* **1970**, *1*, 419–24.
[25] K. Kato, *Acta Crystallogr. Sect. B* **1976**, *32*, 764–7.
[26] B. Gatehouse, A. Wadsley, *Acta Crystallogr.* **1964**, *17*, 1545–54.
[27] M. Yang, S. Li, J. Huang, *ACS Appl. Mater. Interfaces* **2021**, *13*, 39501–12.
[28] K. J. Griffith, A. C. Forse, J. M. Griffin, C. P. Grey, *J. Am. Chem. Soc.* **2016**, *138*, 8888–99.
[29] T. Brezesinski, J. Wang, S. H. Tolbert, B. Dunn, *Nat. Mater.* **2010**, *9*, 146–51.
[30] J. Come, V. Augustyn, J. W. Kim, P. Rozier, P.-L. Taberna, P. Gogotsi, J. W. Long, B. Dunn, P. Simon, *J. Electrochem. Soc.* **2014**, *161*, A718–A25.
[31] Z. Zhou, S. Lou, X. Cheng, B. Cui, W. Si, F. Ding, Y. Ma, P. Zuo, C. Du, J. Wang, *ChemistrySelect* **2020**, *5*, 1209–13.
[32] M. P. F. Graça, A. Meireles, C. Nico, M. A. Valente, *J. Alloys Compd.* **2013**, *553*, 177–82.
[33] M. R. N. Soares, S. Leite, C. Nico, M. Peres, A. J. S. Fernandes, M. P. F. Graça, M. Matos, R. Monteiro, T. Monteiro, F. M. Costa, *J. Eur. Ceram. Soc.* **2011**, *31*, 501–6.
[34] M. Liu, C. Yan, Y. Zhang, *Sci. Rep.* **2015**, *5*, 8326.
[35] A. L. Viet, M. Reddy, R. Jose, B. Chowdari, S. Ramakrishna, *J. Phys. Chem. C* **2010**, *114*, 664–71.
[36] J. Meng, Q. He, L. Xu, X. Zhang, F. Liu, X. Wang, Q. Li, X. Xu, G. Zhang, C. Niu, Z. Xiao, Z. Liu, Z. Zhu, Y. Zhao, L. Mai, *Adv. Energy Mater.* **2019**, *9*, 1802695.
[37] L. Kong, X. Cao, J. Wang, W. Qiao, L. Ling, D. Long, *J. Power Sources* **2016**, *309*, 42–9.
[38] S. Li, Q. Xu, E. Uchaker, X. Cao, G. Cao, *CrystEngComm* **2016**, *18*, 2532–40.
[39] Y. Zhou, K. Liu, Y. Zhou, J.-h. Ni, A.-c. Dou, M.-r. Su, Y.-j. Liu, *J. Cent. South Univ.* **2021**, *27*, 3625–36.
[40] C. Shi, K. Xiang, Y. Zhu, W. Zhou, X. Chen, H. Chen, *Ceram. Int.* **2017**, *43*, 12388–95.
[41] M. Wei, K. Wei, M. Ichihara, H. Zhou, *Electrochem. Commun.* **2008**, *10*, 980–3.
[42] G. Liu, B. Jin, K. Bao, H. Xie, J. Guo, X. Ji, R. Zhang, Q. Jiang, *Int. J. Hydrogen Energy* **2017**, *42*, 6065–71.
[43] L. Kong, C. Zhang, J. Wang, W. Qiao, L. Ling, D. Long, *ACS Nano* **2015**, *9*, 11200–8.
[44] V. Augustyn, J. Come, M. A. Lowe, J. W. Kim, P. L. Taberna, S. H. Tolbert, H. D. Abruna, P. Simon, B. Dunn, *Nat. Mater.* **2013**, *12*, 518–22.
[45] H. Zhang, Y. Wang, P. Liu, S. L. Chou, J. Z. Wang, H. Liu, G. Wang, H. Zhao, *ACS Nano* **2016**, *10*, 507–14.
[46] P. Barnes, Y. Zuo, K. Dixon, D. Hou, S. Lee, Z. Ma, J. G. Connell, H. Zhou, C. Deng, K. Smith, E. Gabriel, Y. Liu, O. O. Maryon, P. H. Davis, H. Zhu, Y. Du, J. Qi, Z. Zhu, C. Chen, Z. Zhu, Y. Zhou, P. J. Simmonds, A. E. Briggs, D. Schwartz, S. P. Ong, H. Xiong, *Nat. Mater.* **2022**, *21*, 795–803.
[47] N. Li, X. Lan, L. Wang, Y. Jiang, S. Guo, Y. Li, X. Hu, *ACS Appl. Mater. Interfaces* **2021**, *13*, 16445–53.

[48] I. Andoni, J. M. Ziegler, G. Jha, C. A. Gadre, H. Flores-Zuleta, S. Dai, S. Qiao, M. Xu, V. T. Chen, X. Pan, R. M. Penner, *ACS Appl. Energ. Mater.* **2021**, *4*, 6542–52.

[49] J. Lin, S. Zhao, T. G. Tranter, Z. Zhang, F. Peng, D. Brett, R. Jervis, P. R. Shearing, *Electrochim. Acta* **2023**, *443*, 141983.

[50] B. M. Patterson, N. L. Cordes, K. Henderson, J. C. E. Mertens, A. J. Clarke, B. Hornberger, A. Merkle, S. Etchin, A. Tkachuk, M. Leibowitz, D. Trapp, W. Qiu, B. Zhang, H. Bale, X. Lu, R. Hartwell, P. J. Withers, R. S. Bradley, *Exp. Mech.* **2016**, *56*, 1585–97.

[51] S. J. Cooper, D. S. Eastwood, J. Gelb, G. Damblanc, D. J. L. Brett, R. S. Bradley, P. J. Withers, P. D. Lee, A. J. Marquis, N. P. Brandon, P. R. Shearing, *J. Power Sources* **2014**, *247*, 1033–9.

[52] T. M. M. Heenan, I. Mombrini, A. Llewellyn, S. Checchia, C. Tan, M. J. Johnson, A. Jnawali, G. Garbarino, R. Jervis, D. J. L. Brett, M. Di Michiel, P. R. Shearing, *Nature* **2023**, *617*, 507–12.

[53] X. Lu, A. Bertei, D. P. Finegan, C. Tan, S. R. Daemi, J. S. Weaving, K. B. O'Regan, T. M. M. Heenan, G. Hinds, E. Kendrick, D. J. L. Brett, P. R. Shearing, *Nat. Commun.* **2020**, *11*, 2079.

[54] W. Du, Z. Zhang, F. Iacoviello, S. Zhou, R. E. Owen, R. Jervis, D. J. L. Brett, P. R. Shearing, *ACS Appl. Mater. Interfaces* **2023**, *15*, 14196–205.

[55] S. R. Daemi, X. Lu, D. Sykes, J. Behnsen, C. Tan, A. Palacios-Padros, J. Cookson, E. Petrucco, P. J. Withers, D. J. L. Brett, P. R. Shearing, *Mater. Horiz.* **2019**, *6*, 612–7.

[56] S. R. Daemi, C. Tan, T. Volkenandt, S. J. Cooper, A. Palacios-Padros, J. Cookson, D. J. L. Brett, P. R. Shearing, *ACS Appl. Energ. Mater.* **2018**, *1*, 3702–10.

[57] A. V. Llewellyn, A. Matruglio, D. J. Brett, R. Jervis, P. R. Shearing, *Condens. Matter* **2020**, *5*, 75.

[58] F. Liu, Z. Zhu, Y. Chen, J. Meng, H. Wang, R. Yu, X. Hong, J. Wu, *ACS Appl. Mater. Interfaces* **2022**, *14*, 49865–74.

[59] A. S. Menon, N. Shah, J. A. Gott, E. Fiamegkou, M. J. Ogley, G. J. P. Fajardo, N. Vaenas, I. Ellis, P. Malliband, G. West, *ChemRxiv.* **2023**.

[60] T. Li, G. Nam, K. Liu, J.-H. Wang, B. Zhao, Y. Ding, L. Soule, M. Avdeev, Z. Luo, W. Zhang, T. Yuan, P. Jing, M. G. Kim, Y. Song, M. Liu, *Energy Environ. Sci.* **2022**, *15*, 254–64.

[61] T. Jousseaume, J. F. Colin, M. Chandesris, S. Lyonnard, S. Tardif, *ACS Energy Lett.* **2023**, *8*, 3323–9.

[62] D. Chen, J. H. Wang, T. F. Chou, B. Zhao, M. A. El-Sayed, M. Liu, *J. Am. Chem. Soc.* **2017**, *139*, 7071–81.

[63] A. J. Merryweather, Q. Jacquet, S. P. Emge, C. Schnedermann, A. Rao, C. P. Grey, *Nat. Mater.* **2022**, *21*, 1306–13.

[64] S. S. Pandurangi, D. S. Hall, C. P. Grey, V. S. Deshpande, N. A. Fleck, *J. Electrochem. Soc.* **2023**, *170*, 050531.

[65] H. C. W. Parks, A. M. Boyce, A. Wade, T. M. M. Heenan, C. Tan, E. Martínez-Pañeda, P. R. Shearing, D. J. L. Brett, R. Jervis, *J. Mater. Chem. A* **2023**, *11*, 21322–32.

[66] A. M. Boyce, E. Martínez-Pañeda, A. Wade, Y. S. Zhang, J. J. Bailey, T. M. M. Heenan, D. J. L. Brett, P. R. Shearing, *J. Power Sources* **2022**, *526*, 231119.

[67] M. Wang, D. Dang, A. Meyer, R. Arsenault, Y.-T. Cheng, *J. Electrochem. Soc.* **2020**, *167*, 100518.

[68] M. N. AL-Shroofy, PhD Thesis, University of Kentucky (US) **2017**.

REVIEW

Dr. J. Lin, Dr. S. Zhao, Dr. R. Jervis*, Prof. P. Shearing*

1 – 16

Probing the Electrochemical Processes of Niobium Pentoxides (Nb₂O₅) for High-Rate Lithium-ion Batteries: A Review

Niobium pentoxide (Nb_2O_5) is a promising high-rate anode material for lithium-ion batteries (LIBs) with extraordinary rate performance beyond 5 C and good theoretical capacity ($\sim$202 mAh g^{-1}). This paper summarizes the state-of-the-art research on Nb_2O_5 polymorphs for LIBs, with an emphasis on the advanced characterisation techniques that have been used to probe the electrochemical processes of Nb_2O_5. Key findings related to Nb_2O_5 that have emerged from the previous studies are highlighted, and new scientific questions that are important for its scale-up and commercialization are proposed for future research.